Supporting Information

Gradient crystallinity and its influence on the poly(vinylidene fluoride)/poly(methyl methacrylate) membrane-derived by immersion precipitation method

Sanjay Remanan[a], Sabyasachi Ghosh[a], Tushar Kanti Das[a], Maya Sharma[b], Madhuparna Bose[c], Suryasarathi Bose[d], Amit Kumar Das[c], Narayan Chandra Das*[a]

[a]Rubber Technology Centre, Indian Institute of Technology, Kharagpur-721302, India

[b]Soft Matter Rheology and Technology division, department of chemical engineering, KU Leuven-3001,

Belgium

[c]Department of Biotechnology, Indian Institute of Technology, Kharagpur-721302, India

[d]Department of Materials Engineering, Indian Institute of Science, Bangalore-560012, India

*Correspondence to: Narayan Chandra Das (E-mail: *ncdas@rtc.iitkgp.ernet.in*)

Contents

List of figures

Figure S4: X-ray diffractogram of the nanoparticles: (a) TiO_2 and (b) GO nanosheets.

Figure S5: FT-IR spectra of the prepared PVDF and blend membranes.

Figure S6: Lorentz corrected Kratky plot of PVDF-PMMA blend.

Figure S7: Small angle X-ray scattering of 70/30 nanocomposite membranes.

Figure S8: One-dimensional correlation function of the 70/30 neat and nanocomposite membrane with variation in filler concentration.

Figure S9: X-ray micro-CT of the prepared PVDF membrane (a) 3D structure, (b) cross-sectional morphology.

Figure S10: Cross-sectional morphology of 70/30+5wt% nanocomposite membrane showing the aggregation of fillers on the top surface.

Figure S11: Energy dispersive spectra of the 70/30 nanocomposite membranes: (a&a_1) 3wt% and (b&b_1) 5wt%.

Figure S12: Antifouling nature of the membrane studied through FRR and IFR.

Figure S13: Membrane compaction of the neat 70/30 and with 5wt% filler was measured in the cross-flow filtration system.

Wet tensile strength of the blend membranes

Tensile strength of the membranes was measured in the wet condition to investigate the practicability during the filtration study. PVDF membranes show maximum tensile strength, as shown in Figure S1. Addition of the second polymer such as PMMA has a profound influence in the membrane mechanical property leads to the decrement in the tensile strength when the PMMA concentration is more than 30wt%. This decrease is observed from the thermodynamic instability during the liquid to solid phase separation and decrease in the percentage crystallinity. Neat PVDF membrane has high crystallinity, which was studied in the DSC and XRD analysis, and crystalline material has high tensile strength. During

the application of tensile stress uncoiling of the polymer chains in the amorphous region initiates first followed by the separation of ordered chains in the crystallites which are held together by the tie chains. The neat PVDF membrane breaks when the tie chains start to rupture[1]. Also, membrane pores contribute to the stress concentration, which is significant in the 60/40 blend leads to the membrane breakage[2,3]. Introduction of glassy polymers hinders the crystallinity of PVDF, increases the membrane porosity, which severely decreases the tensile strength. During the crossflow filtration study, 60/40 membranes break many times in the test cell, possibly due to the less tensile strength. Hence, the wet tensile strength of the membrane was tuned by the concentration of the second polymer (PMMA) in the PVDF matrix.

Preparation of the graphene oxide (GO) nanosheets

Graphene oxide was prepared by the modified Hummers method as reported elsewhere [4,5]. Briefly, 1g of graphite flakes were dispersed in the 55:6.5 mL of H_2SO_4:H_3PO_4 solution in an ice bath and kept stirred by a magnetic stirrer for half an hour. The oxidant $KMnO_4$ was then introduced into the reaction mixture for the oxidation of graphite and kept stirring the mixture for three days at 25˚C, $H_2O_2$was added to stop the reaction. The synthesized graphitic oxide then washed with 1M HCl and distilled water for three days. The GO was collected by centrifugation at 10,000 rpm for 45 minutes and washed several times until the pH of the supernatant reaches ~7. Obtained GO was vacuum dried for several days at ambient temperature and then at 40 ºC for a week.

Preparation of the titanium dioxide (TiO_2) nanoparticle

TiO_2 nanoparticle was synthesized by sol-gel method as shown schematically in **Figure S2**[6,7]. Tetrabutylorthotitanate ($TiOBu_4$) was used as the precursor material and was reacted with

ethanol, water, and nitric acid in the ratio of 1:20:6:0.8. Initially, $TiOBu_4$ was dissolved in ethanol and continued stirring for 10 minutes. Then HNO_3 was added and continued the stirring for next 30 minutes.

To the above solution, 16.7 ml of ethanol followed by 1.5 ml of H_2O were added slowly. The amalgam then hydrolyzed at ambient temperature with vigorous magnetic stirring until the formation of a translucent gel. The prepared sol was then taken for ageing at room temperature for two days. The obtained gel was dried at 100 ºC for 24 hours and finally calcinated in a silica crucible at 400 °C for three hours.

Fourier Transform Infrared Spectroscopy (FT-IR) analysis of the membranes

FT-IR spectrum of the prepared membrane was shown in Figure S5. The peaks appeared at 612, 763, 795 and 975 cm^{-1} are respectively CF_2 bending, CF_2 skeletal bending, CH_2 rocking and CH_2 twisting and these are characteristic α-phase. The presence of α phase was also confirmed by the XRD analysis. The peak appeared at 843, and 1180 is tending to represent the γ phase of the PVDF and could be the mixture of α and γ crystalline phase of the membrane formed after phase inversion [8].

The peak appeared at 2951, 1724 and 1439 cm^{-1} in the blend samples are respectively C-O-CH_3 stretching, C=O stretching and CH_2 scissoring of PMMA polymer. Also, the peak appeared at 1400, 1271 and 1072 cm^{-1} are the deformed vibrations of CH_2 groups in the PVDF polymer [9]. The solvent used for the dope solution affects the crystalline phases of the final membrane formed during precipitation. Tao et al.[10] found that a good solvent for the PVDF can form α-phase during the precipitation while as partially dissolved solvents form β-phase in PVDF membrane.

Supporting figures

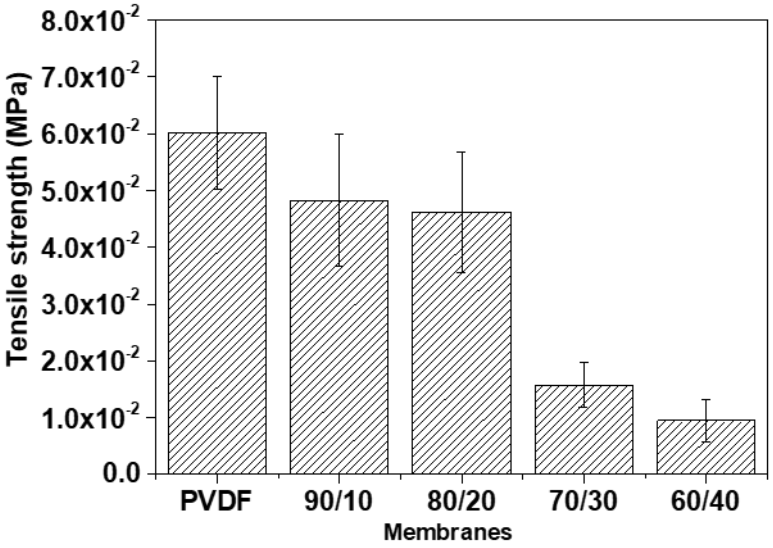

Figure S1: Wet tensile strength of the membrane measured in the UTM.

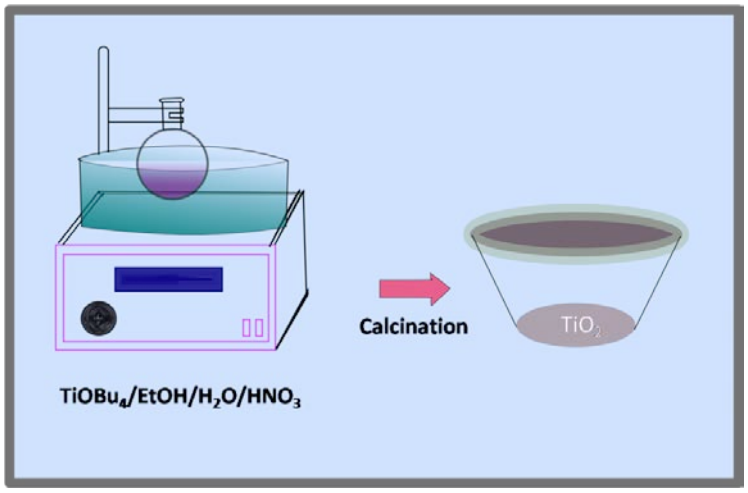

Figure S2: schematic representation of TiO_2 nanoparticle preparation.

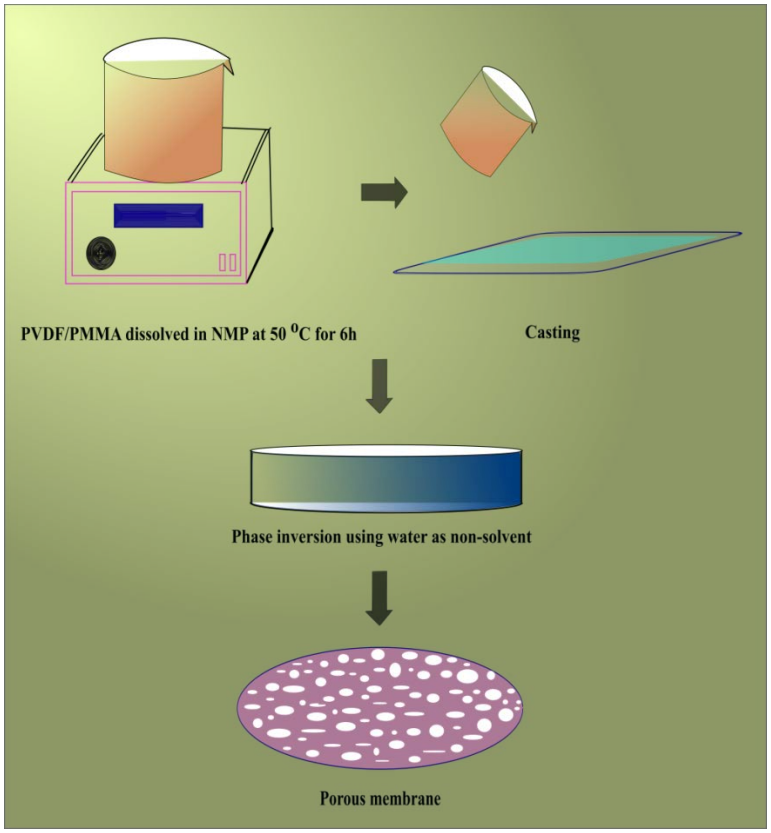

Figure S3: Schematic of PVDF/PMMA membrane preparation by non-solvent induced phase separation (NIPS) method.

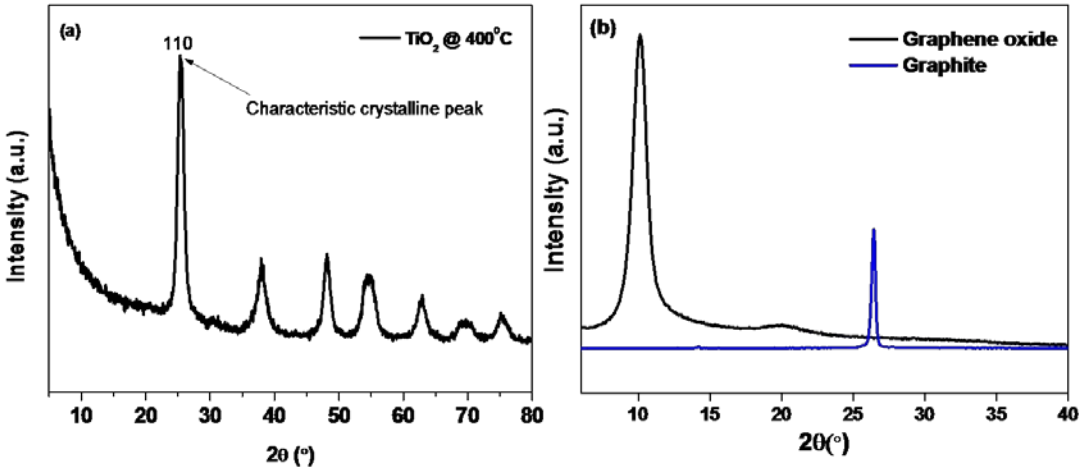

Figure S4: X-ray diffractogram of the nanoparticles: (a) TiO_2 and (b) GO nanosheets and graphite particles.

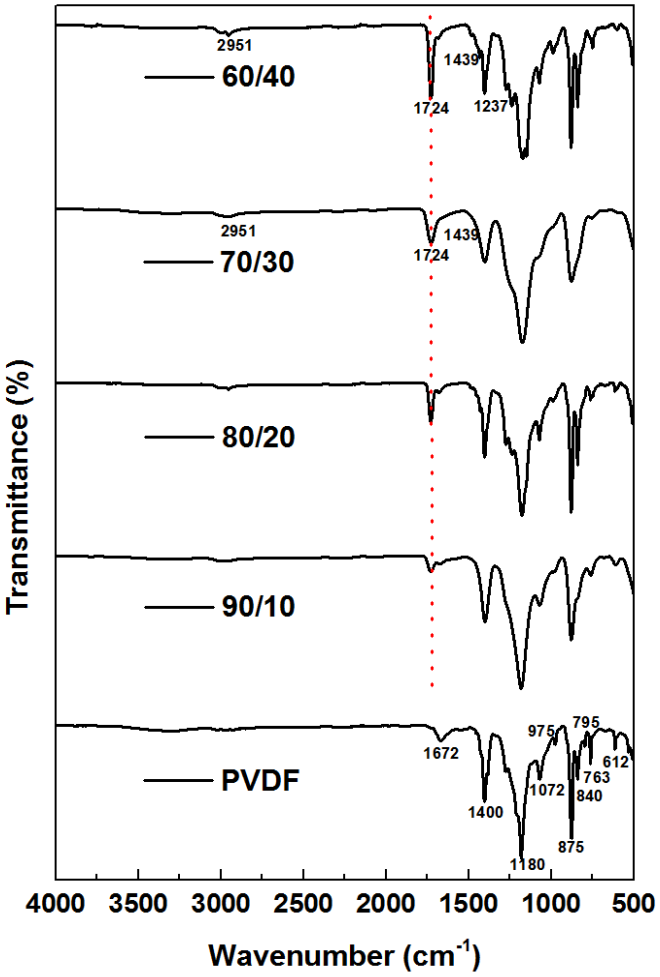

Figure S5: FT-IR spectra of the prepared PVDF and blend membranes.

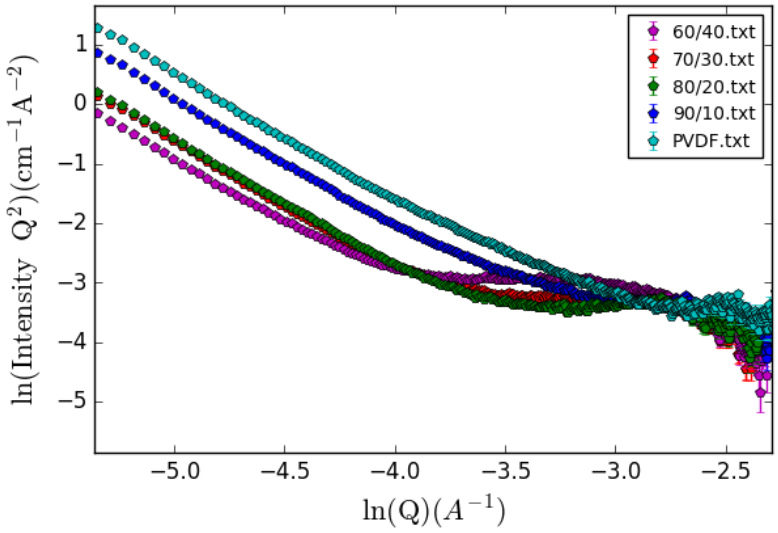

Figure S6: Lorentz corrected Kratky plot of PVDF-PMMA blend membranes plotted in the log-log scale.

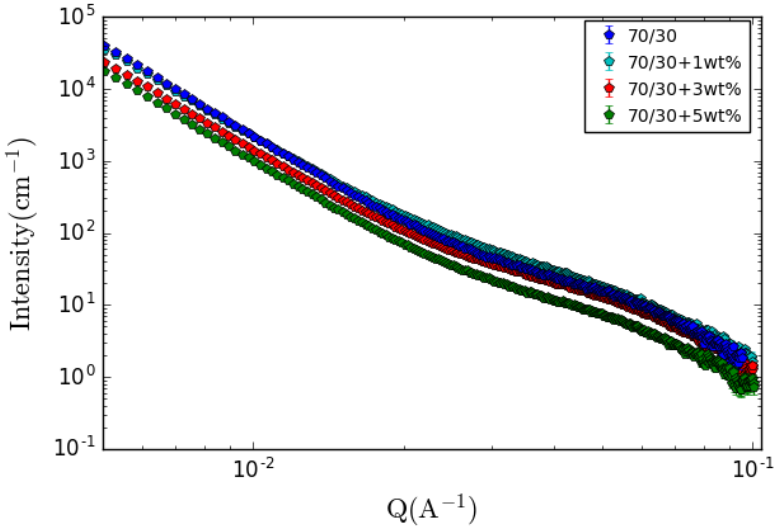

Figure S7: Small angle X-ray scattering of 70/30 nanocomposite membranes.

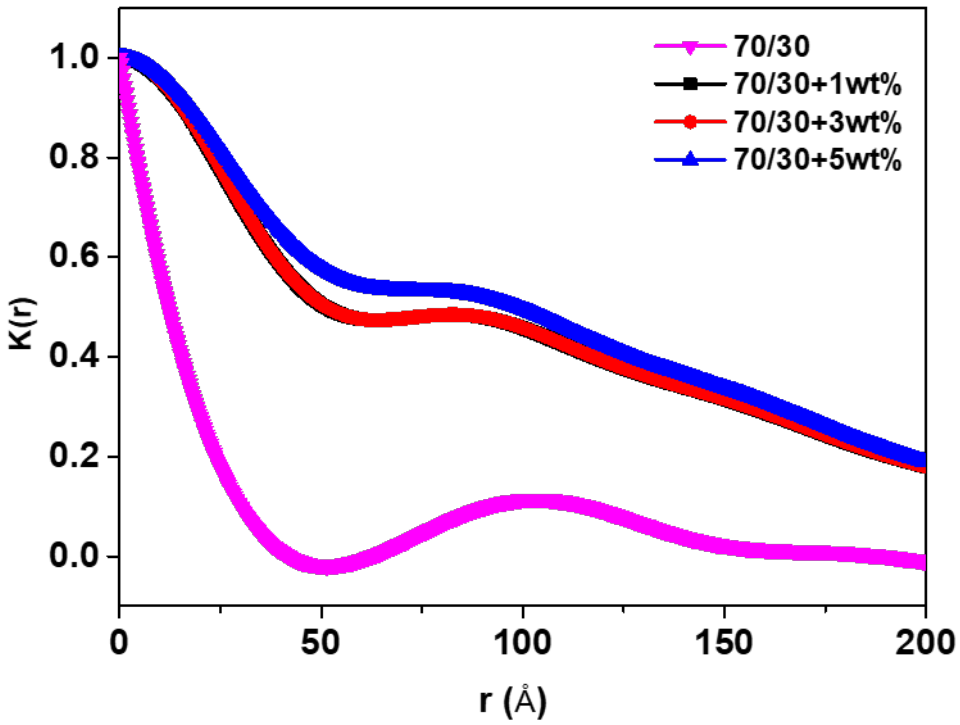

Figure S8: One-dimensional correlation function of the 70/30 neat and nanocomposite membrane with variation in filler concentration.

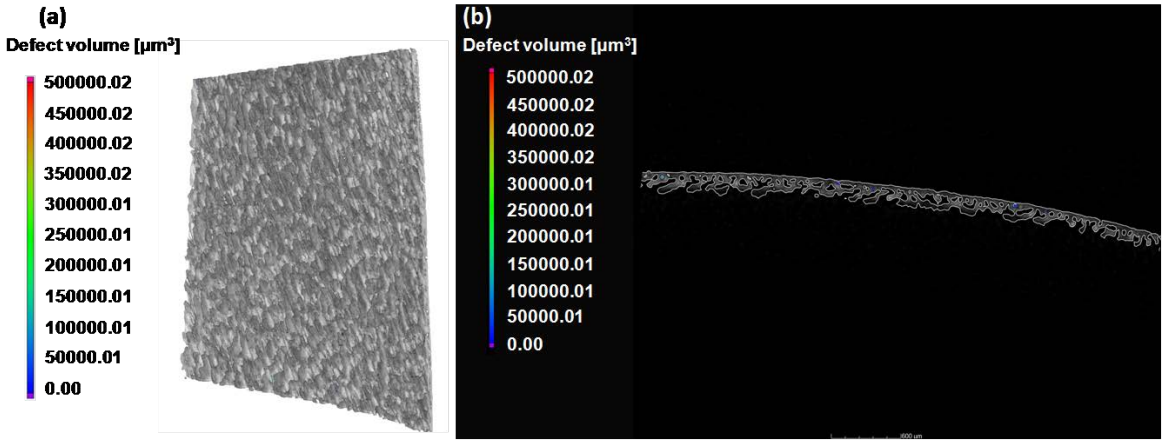

Figure S9: X-ray micro-CT of the prepared PVDF membrane (a) 3D structure, (b) cross-sectional morphology.

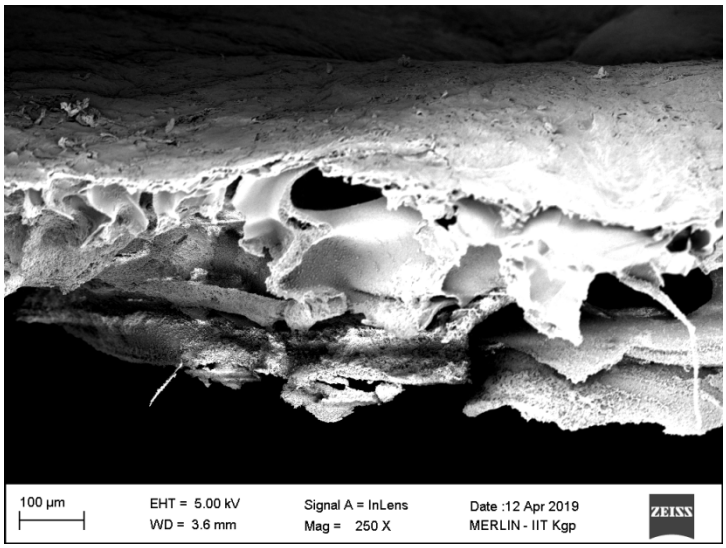

Figure S10: Cross-sectional morphology of 70/30+5wt% nanocomposite membrane showing the aggregation of fillers on the top surface.

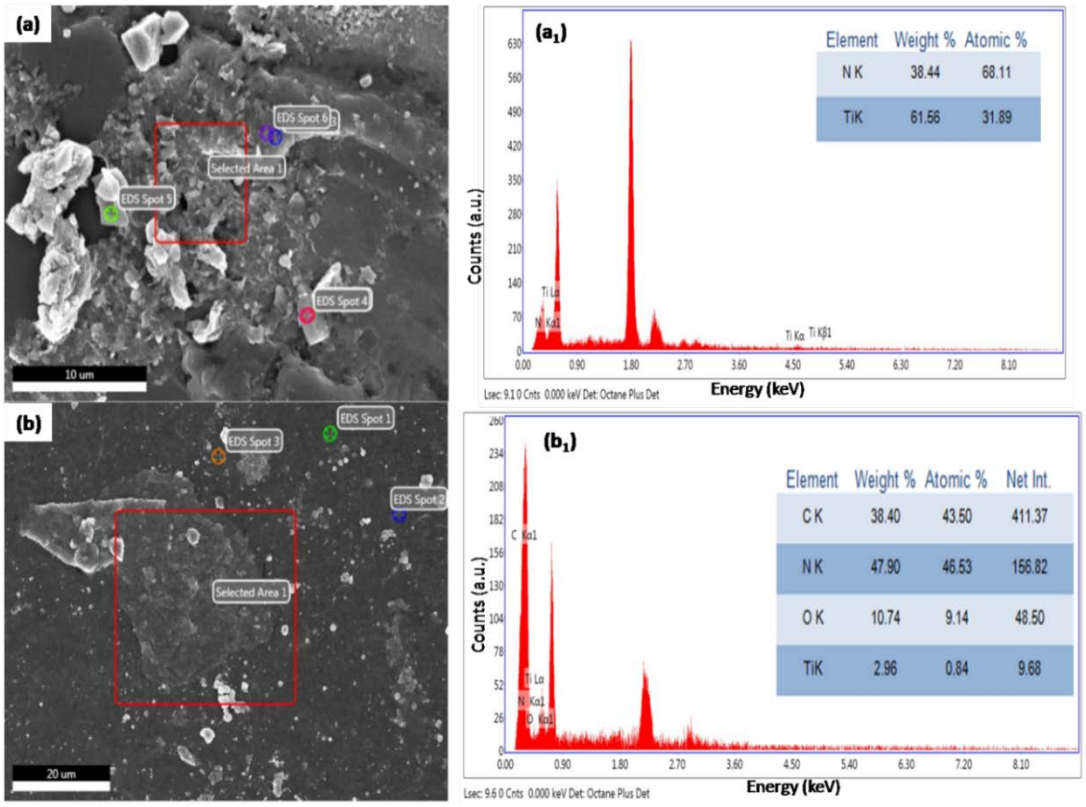

Figure S11: Energy dispersive spectra of the 70/30 nanocomposite membranes: (a&a_1) 3wt% and (b&b_1) 5wt%.

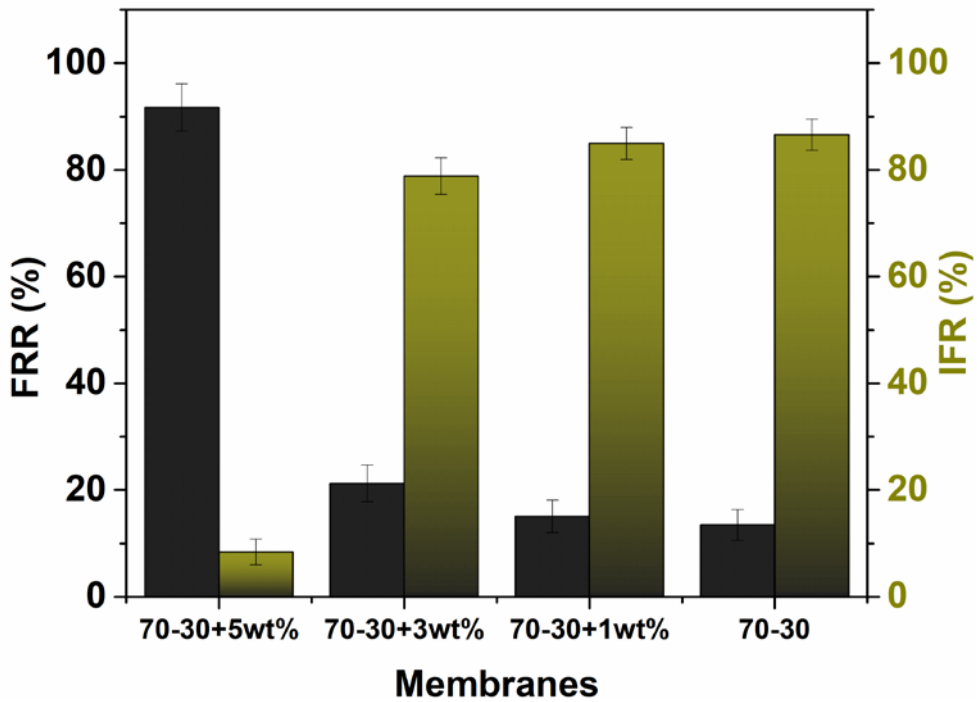

Figure S12: Antifouling nature of the membrane studied through FRR and IFR.

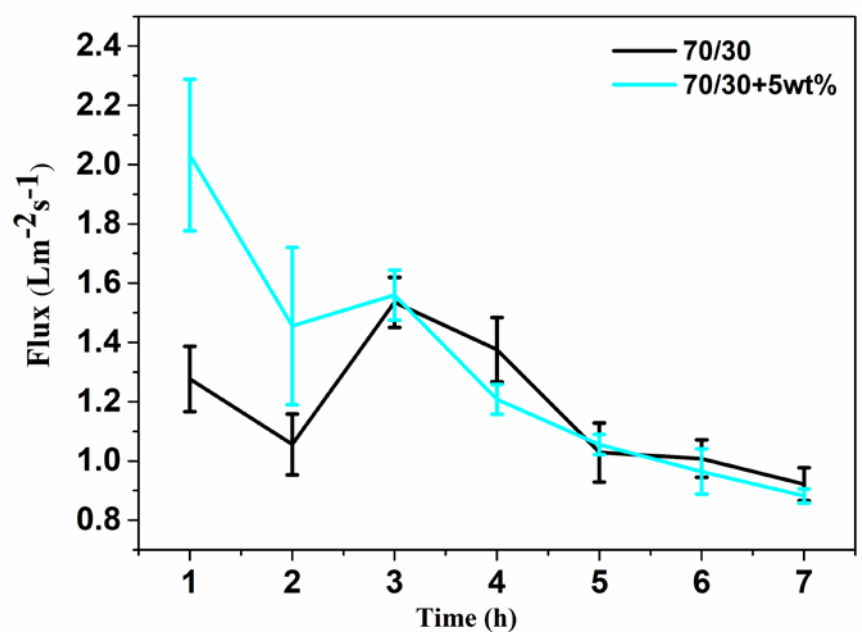

Figure S13: Membrane compaction of the neat 70/30 and with 5wt% filler was measured in the cross-flow filtration system.

References

1. Callister, W. D.; Rethwisch, D. G., Materials science and engineering: an introduction; John wiley & sons New York, 2007.
2. Ma, Y.; Shi, F.; Ma, J.; Wu, M.; Zhang, J.; Gao, C., Desalination 272, 51 2011.
3. Panda, S. R.; De, S., Journal of polymer research 20, 179 2013.
4. Kumar, S.; Raj, S.; Sarkar, K.; Chatterjee, K., Nanoscale 8, 6820 2016.
5. Mural, P. K. S.; Jain, S.; Kumar, S.; Madras, G.; Bose, S., Nanoscale 8, 8048 2016.
6. Wang, Q.; Xu, S.; Shen, F., Applied Surface Science 257, 7671 2011.
7. Hu, L.; Song, H.; Pan, G.; Yan, B.; Qin, R.; Dai, Q.; Fan, L.; Li, S.; Bai, X., Journal of Luminescence 127, 371 2007.
8. Sharma, M.; Madras, G.; Bose, S., Physical Chemistry Chemical Physics 16, 14792 2014.
9. Sharma, M.; Sharma, K.; Bose, S., The Journal of Physical Chemistry B 117, 8589 2013.
10. Tao, M.-m.; Liu, F.; Ma, B.-r.; Xue, L.-x., Desalination 316, 137 2013.